Chemical Engineering Science 205 (2019) 83–93

Contents lists available at ScienceDirect

Chemical Engineering Science

journal homepage: www.elsevier.com/locate/ces

Rise of Taylor bubbles through power law fluids – Analytical modelling and numerical simulation

Arijit Majumdar, P.K. Das *

Mechanical Engineering Department, Indian Institute of Technology, Kharagpur, WB 721302, India

HIGHLIGHTS

- Semi-analytical model for predicting rise velocity of Taylor bubble in power law fluid.
- Numerical simulation for Taylor bubble rise in a power law fluid using VOF method.
- Effect of n and K on dynamics of Taylor bubble.
- Influence of surface tension on the shape of bubble tail only.
- Pronounced effect of n on shape and speed of the bubble.

ARTICLE INFO

Article history:
Received 8 December 2018
Received in revised form 27 March 2019
Accepted 13 April 2019
Available online 17 April 2019

Keywords:
Taylor bubble
Power law fluid
VOF
Rise velocity
Semi-analytical theory

ABSTRACT

An attempt has been made to explore the dynamics of Taylor bubbles rising through circular tubes filled with stagnant power law fluids using CFD and a semi-analytical technique. While the freeware OpenFOAM was used for CFD simulation, the semi-analytical model was developed considering viscous film drainage around the axisymmetric bubble and was closed using a single tuning coefficient from experimental data. Bubble rise velocity derived from both the techniques exhibit good agreement with experiments. Though the velocity field around a bubble rising through a power law fluid does not show any remarkable difference with that observed for bubbles through Newtonian liquids, the rise velocity is noted to depend strongly on both K and n of the power law relationship. Nevertheless, the influence of n is much greater as is evident from the change of nose shape with its variation. Effect of such variation in nose shape is also reflected in the predicted rise velocity. However, as observed in case of Newtonian fluids, for a given n and K, the rise velocity of Taylor bubble asymptotically reaches a constant value as the bubble volume is increased. It is also seen that surface tension does not have any significant effect on the nose shape and rise velocity while it modifies the tail shape. Finally, it has been noted that the increase in rise velocity with tube diameter depicts a non linear trend for non-Newtonian fluids while it is linear for their Newtonian counterpart.

1. Introduction

Gas liquid two phase flow is characterized by the presence of dynamic interfacial structures. During such flow through closed conduits, elongated bubbles of a typical shape, known as Taylor bubbles, are often encountered. Taylor bubbles have a blunt, bullet shaped nose followed by a slender body separated from the surrounding wall only by a thin liquid film. The tail of the Taylor bubble can be convex, concave, flat or jagged depending upon the operating condition and the liquid properties. Taylor bubble are not only seen rising through a stationary liquid due to buoyancy but are also observed in cocurrent and counter current flow through a wide range of tube diameters for a wide variation of phase flow rates.They exhibit a noticeable change in shape depending on the properties of the surrounding liquid. Downward transport of elongated liquid drops termed as Taylor drops, is also possible and a heavier liquid mass falling through a lighter one shows many attributes typical to a commonly known rising Taylor bubble (Mandal et al., 2008). Fluid properties, particularly liquid viscosity has a unique effect on the shape of the bubble. Fig. 1 depicts Taylor bubbles of comparable volume rising through three stagnant liquids water, glycerine and silicon oil respectively, contained in tubes of 19 mm diameter.

Taylor bubbles are mostly observed during slug flow where they appear in alternate successions being separated by liquid

* Corresponding author.
E-mail address: pkd@mech.iitkgp.ac.in (P.K. Das).

https://doi.org/10.1016/j.ces.2019.04.028
0009-2509/

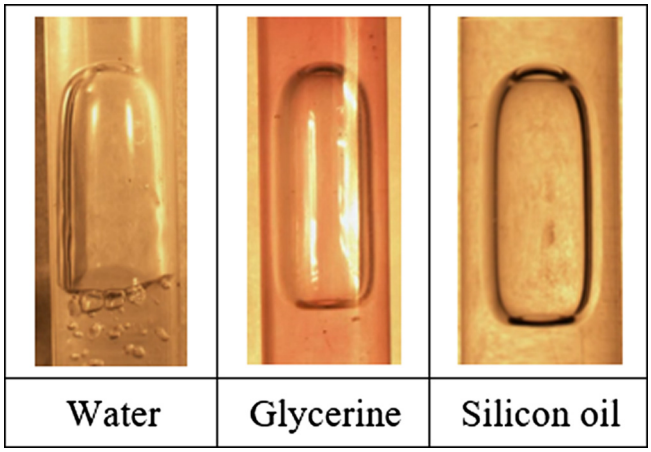

Fig. 1. Taylor bubble rising through different liquids.

slugs. Prediction, analysis and control of slug flow are essential in several industrial processes such as oil and gas transport in wells, air-lift reactors, activated sludge processes, pipeline transportation, polymer devolatilization, coating technology, heat exchangers and many more. Moreover, slug flow occurs over a wide range of flow properties through conduits of narrow cross sections. In all these cases an understanding of the dynamics and hydrodynamics of a Taylor bubble is essential.

Over the years, a large volume of research endeavours, comprising of analytical, experimental and computational techniques have been made to investigate several aspects of Taylor bubble motion. The shape and hydrodynamics of a bubble are implicitly related. Taylor bubbles are also no exception. All the theories pertaining to Taylor bubble motion, therefore, establishes its dynamics with respect to its typical shape.

Some of the early analytical modelling of Taylor bubble was proposed by Davies et al. (1988) and Dumitrescu (1943) based on several assumptions. The key of them being the apriori assumption of the shape of the bubble nose. They determined the terminal velocity of the bubble assuming the bubble nose to be a part of a sphere and the surrounding liquid to be ideal which enables the use of velocity potential as well as Bernoulli's theorem. Later comprehensive analyses were performed theoretically (Batchelor, 1987; Batchelor, 2000; Bendiksen, 1985; Collins et al., 1978; Funada et al., 2005; Reinelt, 1987) by relaxing many of these assumptions. Goldsmith and Mason (1962) and Brown (1965) studied the falling film around the bubble by considering the effect of viscosity. The effect of interfacial tension on bubble velocity was considered by Wallis. He proposed a function of Eötvös number to account for the surface tension. Zudin (2013) gave an analytical solution using superposition of elementary flows.

White and Beardmore (1962) performed a large number of experiments on rising Taylor bubbles in a circular tube by varying the tube diameter and the relevant fluid properties such as viscosity, surface tension and density. They used Froude number (Fr), Eötvös number (Eo) and Morton number (Mo) as the influencing parameters and gave a general graphical correlation. Zukoski (1966) observed that the effect of viscosity on the bubble velocity becomes negligible at Reynolds number greater than 200. Campos and Carvalho (1988) analyzed the flow near the wake region of a Taylor bubble and identified laminar, transitional and turbulent fluid flow at the wake. They suggested that the flow near the wake depends on the inverse viscosity number $N_f = \rho_L g^{1/2} D^{3/2} / \mu_L$. The analysis by Brown (1965) was extended by Mandal et al. (2008) for the case of liquid Taylor drops where they gave a semi-empirical equation for the bubble terminal velocity. Over the years, a large number of correlations have been proposed to predict the rise velocity of Taylor bubble through Newtonian fluid. Such correlations try to incorporate the effect of viscosity, surface tension, length of the bubble, velocity of the liquid phase, cross sectional shape of the conduit, etc. Out of such correlations, the one by Viana et al. (2003) for rise of Taylor bubble through liquid filled round tubes is most comprehensive. Similarly a number of correlations are also available for the film thickness of Taylor bubble through circular tubes filled with Newtonian fluid (Kang et al., 2010; Llewellin et al., 2012). However no correlation have been proposed for non-Newtonian fluids.

Mao et al. (1990) made one of the earliest efforts to computationally model the rising axisymmetric Taylor bubbles. They adjusted the bubble interface for the normal stress to satisfy the constant pressure criteria inside the bubble. Bugg et al. (1998) studied several important features of Taylor bubble such as terminal velocity and film thickness using the Volume of Fluid (VOF) method. Two dimensional simulations of gaseous Taylor bubble, using the VOF method, rising in counter current flow were performed by Figueroa-Espinoza and Fabre (2011). They reported a critical downward flow rate of liquid beyond which the bubble becomes asymmetric and rises faster. Recently Lu et al. (2009) used a front tracking method to study the rising axisymmetric Taylor bubbles.

The vast literature available on the motion of the Taylor bubble considered its movement through Newtonian fluids almost without an exception. Though non-Newtonian fluids are very common in many industrial and biological systems, information about the motion of Taylor bubbles in non-Newtonian fluid is really meagre. It is an established fact that the rheology of the surrounding liquid strongly influences the shape of the nose, tail and the thickness of the liquid film surrounding the Taylor bubble. It also goes without saying that the velocity of a Taylor bubble is a function of its viscosity. Nevertheless, the efforts to understand the dynamics of Taylor bubble through a non-Newtonian fluid is not only few in number but are also disjointed. Carew et al. (1995) gave a semi-theoretical expression for the terminal velocity of the bubble in an inclined cylindrical tube. Kaml et al. (2003) derived one-dimensional equations for flow of long bubble in power law fluid through cylindrical tube by asymptotic method. He proposed that the film thickness increases with increase in power law index. Motion of gas bubble through blood vessel has been studied numerically by Mukundakrishnan et al. (2009), using the front tracking method. They modelled the blood flow as Newtonian fluid as well as using the generalized power law model and analyzed the wall shear stress for different bubble diameters and flow rates. Sousa et al. (2005) performed PIV measurements for Taylor bubble rising in carboxymethylcellulose (CMC) and polyacrylamide (PAA) solutions. Numerical study on Taylor bubble rising in non-Newtonian fluid was done by Arajo et al. (2017). They studied the bubble dynamics in stagnant, co-current and counter current flow.

In the present work, the upward transport of Taylor bubbles through a vertical circular tube filled with stationary power law fluids has been simulated using the Volume of Fluid(VOF) solver *interFoam* of the open source CFD package OpenFOAM. The simulation results predict the shape and terminal velocity of Taylor bubbles and also reveal the effect of the rheological parameters of the fluids on these two important attributes of the rising Taylor bubble. Parallelly, a semi-analytical technique has also been proposed to obtain the terminal bubble velocity in a close form expression. A comparison of the terminal velocities obtained from these two methods and the maximum bubble radius predicted by CFD with the published experimental data for Taylor bubbles rising through CMC solutions (Sousa et al., 2005) and Carbopol 981 solution (Carew et al., 1995) of different concentration through a wide range of tube diameters give a good agreement.

2. Theoretical analysis

This section is divided into two parts. In the first part we discuss the governing equations and implementation of the numerical simulation and in the second part we present an approximate analytical model. For the theoretical analysis of the ascending Taylor bubble under steady state through a stagnant liquid, we assume the bubble to be axisymmetric, the flow to be incompressible and laminar and the phases to be mutually immiscible.

2.1. The computational simulation

The dynamic interface of the bubble has been computationally simulated by the Volume of Fluid (VOF) approach, developed by Hirt et al. (1981). In this method the interface is tracked using a parameter α, the volume fraction of the liquid phase. The value of α is 1 inside the liquid phase and 0 inside the gas phase and it has some intermediate value at the interface.

The governing mass and momentum equations for computing the incompressible two phase flow associated with the ascent of the bubble in one-field formulation are as follows

$$\frac{\partial \rho}{\partial t} + \nabla.(\rho \mathbf{u}) = 0 \tag{1}$$

$$\frac{\partial (\rho \mathbf{u})}{\partial t} + \nabla.(\rho \mathbf{u}\mathbf{u}) = -\nabla p + \nabla.\boldsymbol{\tau} + \rho \mathbf{g} + \mathbf{F}_S \tag{2}$$

Herein $\mathbf{u}$ is the velocity field, p is the pressure, $\boldsymbol{\tau} = \mu(\nabla \mathbf{u} + (\nabla \mathbf{u})^T)$ is the viscous stress tensor and $\mathbf{F}_S$ is the surface tension force acting at the gas–liquid interface.

The fluid properties are given as a function of space and time by

$$\rho(\mathbf{x}, t) = \alpha(\mathbf{x}, t)\rho_L + [1 - \alpha(\mathbf{x}, t)]\rho_G \tag{3}$$

$$\mu(\mathbf{x}, t) = \alpha(\mathbf{x}, t)\mu_L + [1 - \alpha(\mathbf{x}, t)]\mu_G \tag{4}$$

The subscripts L and G denote the liquid and gas phase respectively. As per the power law model the viscosity of the liquid phase μ_L is given by

$$\mu_L = K\dot{\gamma}^{n-1} \tag{5}$$

where $\dot{\gamma} = \sqrt{2D_{ij}D_{ji}}$ is the second invariant of strain rate tensor $\mathbf{D}$, K is the consistency coefficient and n is the power law exponent. For a shear-thinning fluid, $0 < n < 1$; while for a shear-thickening fluid $n > 1$.

Along with these equations, the scalar advection equation for the volume fraction is solved. The openware OpenFOAM has been used for the solution of the equations. Compared to Level Set or Front Tracking, the VOF method suffers from an excessive diffusion at the interface leading to smearing. To improve the resolution of the interface, an interface compression term (Rusche, 2002) is used in *interFoam* which is of the form

$$\frac{\partial \alpha}{\partial t} + \nabla.(\mathbf{u}\alpha) + \nabla.(\alpha(1 - \alpha)\mathbf{u}_r) = 0 \tag{6}$$

where the velocity of the effective fluid and the relative velocity is given by

$$\mathbf{u} = \alpha \mathbf{u}_L + (1 - \alpha)\mathbf{u}_G$$

$$\mathbf{u}_r = \mathbf{u}_L - \mathbf{u}_G$$

The continuum surface force (CSF) of Brackbill et al. (1992) is used to model the surface tension acting at the gas-liquid interface.

An axisymmetric 2-D domain is used to carry out the simulations. The tube is taken as a closed domain with walls at the top and bottom.To initiate the simulation, a cylindrical bubble of uniform cross section is taken. The bubble rises from rest and attains an invariant shape as well as a terminal velocity.

With an uniform mesh, the mesh size is taken as 0.0125D in both the axial and the radial direction for a grid independent result; where D is the tube diameter. A maximum time step of 0.0001s is sufficient to yield a converged solution. No slip and no penetration boundary conditions are imposed on the walls and the computation domain was taken as axisymmetric.

The numerical schemes used are first order accurate in time and second order accurate in space. The Pressure Implicit with Splitting Operator (PISO) algorithm was used to solve the pressure velocity coupling in the momentum equation.

2.2. Analytical solution

Taking the queue from Brown (1965), we have extended the analysis for Taylor bubbles rising through stagnant power law fluids. The ascending bubble is represented as stationary bubble past which the liquid flows down, as shown in Fig. 2. Along with the previously stated assumptions, we further assume the gas viscosity and interfacial tension to be negligible, a creeping flow in the falling liquid film and a negligible pressure gradient along the liquid film. We have taken a moving reference frame such that the bubble appears to be stationary with respect to the frame and the liquid flow has been modelled as flow around a cavity.

By volume conservation of the liquid between section AA and BB (Fig. 2)

$$\pi R^2 U = \pi(R^2 - R_c^2)(U + U_F) \tag{7}$$

where R is the radius of the tube, R_c is the equilibrium radius at the tail of the Taylor bubble, U is the terminal velocity of the bubble and U_F is the terminal film velocity relative to tube wall at BB, a section taken far from the bubble nose.

By rearranging the terms in Eq. (7) we get,

$$UR_c^2 = U_F(R^2 - R_c^2) \tag{8}$$

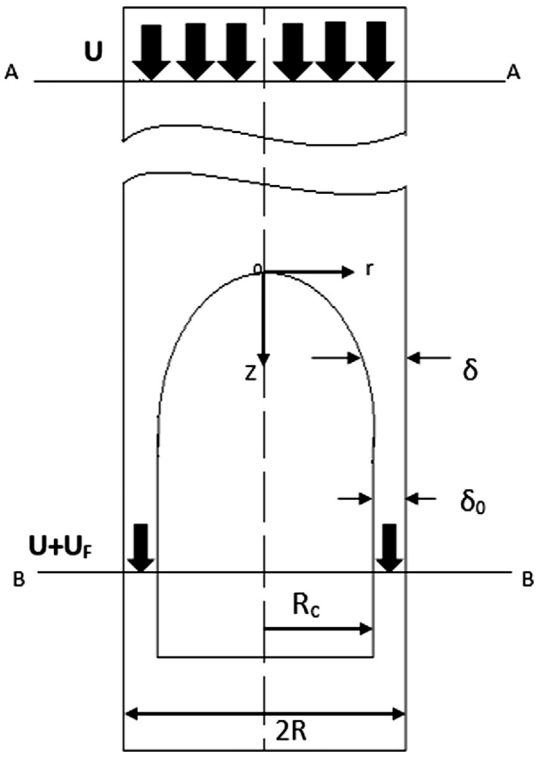

Fig. 2. Coordinate axes used in the analytical model. R is the radius of the tube, δ is the film thickness and R_c is the radius of the bubble body.

A momentum balance for the liquid film is given as follows

$$\frac{1}{r}\frac{\partial(\tau r)}{\partial r} - \rho_L g + \frac{\partial p}{\partial z} = 0 \tag{9}$$

where r is the radial position and τ is the shear stress. The value of pressure gradient $\partial p/\partial z$ is negligible along the film. Thus the equation becomes

$$\frac{1}{r}\frac{\partial(\tau r)}{\partial r} = \rho_L g \tag{10}$$

Integrating Eq. (10) from the bubble interface to any point in the film gives

$$\tau r = \frac{\rho_L g}{2}(r^2 - R_c^2) \tag{11}$$

Here we have assumed the shear stress to be 0 at the bubble interface. For a power law fluid

$$\tau = K\left(\frac{du}{dr}\right)^n \tag{12}$$

where K is the consistency coefficient and n is the power law index. Substituting Eq. (12) in Eq. (11) we get,

$$\left(\frac{du}{dr}\right)^n = \frac{\rho_L g}{2K}\left(r - \frac{R_c^2}{r}\right) \tag{13}$$

$$or, \frac{du}{dr} = \left(\frac{\rho_L g}{2K}\right)^{\frac{1}{n}}\left(r - \frac{R_c^2}{r}\right)^{\frac{1}{n}} \tag{14}$$

Integrating Eq. (14), we have

$$u = \left(\frac{\rho_L g}{2K}\right)^{\frac{1}{n}} \int r^{\frac{1}{n}}\left(1 - \frac{R_c^2}{r^2}\right)^{\frac{1}{n}} dr + C_1 \tag{15}$$

C_1 is the integration constant. In the liquid film $r \sim R$. So, Eq. (15) becomes

$$u \sim \left(\frac{\rho_L g}{2K}\right)^{\frac{1}{n}} \int r^{\frac{1}{n}}\left(1 - \frac{R_c^2}{R^2}\right)^{\frac{1}{n}} dr + C_1 \tag{16}$$

$$u = C\left(\frac{\rho_L g}{2K}\right)^{\frac{1}{n}}\left(1 - \frac{R_c^2}{R^2}\right)^{\frac{1}{n}}\left(\frac{n}{n+1}\right) r^{\frac{n+1}{n}} + C_1 \tag{17}$$

Here C is the proportionality constant. Using the no slip boundary condition at the tube wall the velocity field in the liquid film comes out to be

$$u = C\left(\frac{\rho_L g}{2K}\right)^{\frac{1}{n}}\left[\frac{2\delta}{R} - \left(\frac{\delta}{R}\right)^2\right]^{\frac{1}{n}}\left(\frac{n}{n+1}\right)(r^{\frac{n+1}{n}} - R^{\frac{n+1}{n}}) \tag{18}$$

This gives the average velocity of the liquid in the film from a balance of the volumetric flow rates as

$$\pi U_F(R^2 - R_c^2) = 2\pi \int_{R_c}^{R} urdr \tag{19}$$

By putting Eqs. (8) and (18) in Eq. (19) the terminal velocity of the bubble comes out to be

$$U = \frac{C}{(R-\delta_0)^2}\left(\frac{\rho_L g}{2K}\right)^{\frac{1}{n}}\left[\frac{2\delta_0}{R} - \left(\frac{\delta_0}{R}\right)^2\right]^{\frac{1}{n}}\left(\frac{n}{n+1}\right) \times \left[\left(\frac{2n}{3n+1}\right)\left(R^{\frac{3n+1}{n}} - (R-\delta_0)^{\frac{3n+1}{n}}\right) - R^{\frac{n+1}{n}}\left(R^2 - (R-\delta_0)^2\right)\right] \tag{20}$$

where δ_0 is the equilibrium film thickness.The value of δ_0 is obtained from (Brown, 1965).

$$\delta_0 = \frac{-1 + \sqrt{1 + 4NR}}{2N} \tag{21}$$

The above equation has been derived using a potential flow analysis near the bubble nose, where

$$N = \left[1.81\frac{\rho_L^2 g}{\mu_{eff}^2}\right]^{\frac{1}{3}} \tag{22}$$

the density of the gas phase has been neglected for the evaluation of N. Also we have replaced the fluid viscosity, as given in (Brown, 1965) with effective viscosity μ_{eff}. The value of μ_{eff} has been calculated at the tube wall. According to power law the effective vicosity is given by

$$\mu_{eff} = K\left(\frac{du}{dr}\right)^{n-1}|_{r=R} \tag{23}$$

Putting the expression of du/dr from Eq. (14) and replacing r by R we get

$$\mu_{eff} = K\left(\frac{\rho_L g}{2K}\right)^{\frac{n-1}{n}}\left[R - \frac{(R-\delta_0)^2}{R}\right]^{\frac{n-1}{n}} \tag{24}$$

By simultaneously solving Eqs. (21), (22) and (24) we get the value of the equilibrium film thickness δ_0 and by putting this value in Eq. (20) we obtain the value of U. The expression of U contains C, the constant of proportionality introduced in Eq. (17). Determination of C from the first principle is a formidable task and is not possible in the framework of present analysis. As an alternative, a closure of the present model may be obtained from experimental inputs. Unfortunately, though some experiments on the propagation of Taylor bubble through power law fluids are reported, they do not provide enough information regarding the liquid rheology enabling the application of the analytical solution and the computational simulation. By an extensive literature search we could locate two useful sources. Sousa et al. (2005) have provided experimental data for the rise velocity of Taylor bubble through a tube of internal diameter of 0.032 m filled with different concentrations of CMC solution. Carew et al. (1995) have studied experimentally the rise of Taylor bubble through Carbopol 981 of different concentrations using tubes of three different diameters (0.025 m, 0.045 m, 0.070 m). These studies provide data for rise velocity of taylor bubble for a wide range of power law parameters (K and n) and tube diameter. On comparing our analytical model with experiments of Carew et al. (1995) and Sousa et al. (2005) we get

$$C \simeq 0.738 \tag{25}$$

with sample correlation coefficient $r_{xy} = 0.952$

Finally, the expression for the terminal velocity of the Taylor bubble rising through a power law fluid is obtained as

$$U = \frac{0.738}{(R-\delta_0)^2}\left(\frac{\rho_L g}{2K}\right)^{\frac{1}{n}}\left[\frac{2\delta_0}{R} - \left(\frac{\delta_0}{R}\right)^2\right]^{\frac{1}{n}}\left(\frac{n}{n+1}\right) \times \left[\left(\frac{2n}{3n+1}\right)\left(R^{\frac{3n+1}{n}} - (R-\delta_0)^{\frac{3n+1}{n}}\right) - R^{\frac{n+1}{n}}\left(R^2 - (R-\delta_0)^2\right)\right] \tag{26}$$

3. Results and discussion

In this section, we first validate the terminal velocity and maximum radius of the Taylor bubble obtained from numerical simulations and analytical model against the experimental data reported by Carew et al. (1995) and Sousa et al. (2005) on the motion of Taylor bubble through power law fluids. We also report numerically the effect of bubble volume, surface tension and

power law parameters n and K on the terminal velocity and shape of the bubble obtained from the computational simulation.

3.1. Comparison with experimental results and correlations

We have validated the analytical and numerical results by comparing them with the experimental data reported for different concentrations of CMC (Sousa et al., 2005) and Carbopol (Carew et al., 1995) solution for a range of tube diameters and liquid viscosities (different combinations of n and K).The analytical and numerical results show good agreements with experimental data in Table 1. In the table, we present the power law parameters for different CMC and Carbopol solutions, tube diameters and the terminal velocity of the Taylor bubble obtained numerically and analytically using those parameters along with the associated errors. The values of n and K are obtained by curve fitting from the reported viscosity vs. shear rate plots for CMC solutions (Sousa et al., 2005). For the Carbopol 981 solution we took the values of n and K from (Carew et al., 1995). We have also given the upper limits of viscosity for these fluids μ_{max} which are used in the numerical simulation. At a very low shear rate, the viscosity of CMC and Carbopol solutions become almost constant and they do not obey the power law any longer. To cope with that, we have used the constant value of viscosity (μ_{max}) at low shear rates so that in the simulation, the liquid is treated as Newtonian after the shear rate reaches a critical value.

Table 1 reveals that for CMC solution numerical results predicts the experimental data within five percent error with an exception of a single data with 11.8 percent error. For the analytical solution on the other hand the maximum error is 7.5%. For Carbopol 981 solution the maximum error is within 5% in numerical prediction. In this case the analytical solution exhibit a higher error, the maximum value being around 13%. It may also be noted that the reported experimental errors are 4% and 2% respectively for CMC solution (Sousa et al., 2005) and Carbopol (Carew et al., 1995). Further, the analytical solution is based on a number of assumptions, one of them being, $\delta_0 \ll R$. This is violated for smaller tube diameters and thinner bubbles (high effective viscosity). In this regard, we like to draw attention of the readers to a typical data point of (Carew et al., 1995) which is not included in Table 1. For 0.25% Carbopol solution in 0.025 m diameter tube, our analytical prediction gives 20% error whereas for numerical prediction the error is restricted to 7%. A large film thickness is responsible for this and the example indicates the limitation of the analytical solution. It has been observed in several experiments that the bubbles do not have the maximum radius immediately behind the nose. Based on this fact, we have compared the maximum radius $(r/D)_{max}$ of the bubbles obtained in our numerical simulations with the reported data of (Sousa et al., 2005), as shown in Table 2. The maximum deviation between the experiment and the numerical data is 7.6%. We could not get such information from the other literature. It is also not possible to obtain $(r/D)_{max}$ from our analytical model, since we have considered the bubble to have an equilibrium radius, thereby making the liquid film thickness constant behind the bubble nose (see Fig. 2).

Table 2
Maximum bubble radius $(r/D)_{max}$ for different concentration of CMC solutions.

Conc. of CMC solution	Experiment	Numerical Simulation
0.3%	0.438	0.429
0.4%	0.427	0.426
0.5%	0.418	0.424
0.6%	0.406	0.416
0.8%	0.393	0.403
1.0%	0.353	0.380

There are several correlations for obtaining the equilibrium fim thickness of a Taylor bubble in Newtonian fluid. Based on numerical simulation, Kang et al. (2010) estimated the film thickness of Taylor bubble rising in stationary liquids:

$$\frac{\delta_0}{R} = 0.64 N_f^{-0.2} \tag{27}$$

Here N_f is the inverse viscosity number. Llewellin et al. (2012) used experimental data of their own as well as those from Nogueira et al. (2006) to determine the following empirical correlation:

$$\frac{\delta_0}{R} = 0.204 + 0.123 \tanh(2.66 - 1.15 \log(N_f)) \tag{28}$$

But there are no available correlations for determining the film thickness in case of a non-Newtonian fluid. In our analytical model, we used the correlation given by Brown (1965) (Eq. (21)) by introducing an effective viscocity of the power law fluid. For the sake of comparison, we also tried to evaluate the film thickness and terminal velocity of the Taylor bubble rising in power law fluid from the above mentioned correlations. We evaluated N_f from the following equation:

$$N_f = \frac{\rho_L}{\mu_{eff}} \sqrt{gD^3} \tag{29}$$

where D is the tube diameter and μ_{eff} is the effective viscosity calculated from Eq. (24). We found out that even though the correlations suggested in (Kang et al., 2010 and Llewellin et al., 2012) accurately predict the film thickness of taylor bubble in Newtonian liquid, for a power law fluid these models gave erroneous results

Table 1
Power law model parameters for CMC and Carbopol 981 solutions, tube diameters and terminal velocity of the Taylor bubble through them.

Fluid	Tube dia. (m)	Conc. (%)	n	K	μ_{max} (Pa s)	Rise velocity of Taylor bubble (m/s)				
						Experiment	Numerical		Analytical	
							Value	Error %	Value	Error %
CMC (Sousa et al., 2005)	0.032	0.3	0.772	0.079	0.047	0.198	0.203	2.525	0.191	−3.535
		0.4	0.714	0.175	0.107	0.195	0.202	3.589	0.186	−4.615
		0.5	0.620	0.386	0.187	0.192	0.184	−4.166	0.182	−5.104
		0.6	0.600	0.622	0.347	0.187	0.179	−4.278	0.176	−5.668
		0.8	0.496	1.621	0.995	0.180	0.171	−5.0	0.167	−7.222
		1.0	0.437	4.189	2.799	0.160	0.141	−11.8	0.148	−7.50
Carbopol 981 (Carew et al., 1995)	0.025	0.125	0.485	1.016	0.310	0.141	0.137	-2.837	0.147	4.255
	0.045	0.125	0.485	1.016	0.310	0.202	0.212	4.950	0.217	7.426
		0.25	0.386	2.927	1.912	0.179	0.185	3.352	0.202	12.849
	0.07	0.125	0.485	1.016	0.310	0.266	0.277	4.135	0.283	6.391
		0.25	0.386	2.927	1.912	0.241	0.236	-2.074	0.268	11.203

while the bubble velocity obtained using the correlation of (Brown, 1965) was closer to the experimental data.

It may also be noted that the difference between predictions and the experimental results increases consistently with the increasing concentration of the solutions. This indicates a shift of the liquid properties towards the non-Newtonian behaviour. The non linearity in the stress-strain relationship increases. With the increase in the non-Newtonian behaviour, a gradual shift from the assumed power law rheology can also not be ruled out.

According to power law relationship, the viscosity depends on both K and n. With the increase in concentration of both CMC and Carbopol solution, magnitude of K increases while that of n decreases. The effect of K overshadows the effect of n, with an overall effect of an increase in viscosity of the solution. With the increase in viscosity, the rise velocity of the bubble reduces and there is a thickening of the liquid film surrounding the Taylor bubble. To understand the influence of K and n individually, we have conducted numerical simulation for diffrenent values of n and K, reported in a later section.

3.2. Effect of bubble length

Bubble length is the ratio of the volume of the bubble to the cross sectional area of the tube. Sousa et al. (2006) used PIV measurements to study the effect of bubble length on its terminal velocity for a Taylor bubble rising in CMC solution. They found out that for an open tube, due to the expansion of gas, the bubble velocity increases with increase in bubble length. By suppressing the effect of gas expansion (with the top of the liquid filled tube closed, the velocity of a Taylor bubble is independent of its length.We performed simulations in a closed tube to understand the effect of bubble length on the bubble velocity. With the increase in length, initially the terminal velocity increases and then becomes constant asymptotically. In Fig. 3, the variation of Froude number (Fr) with respect to non-dimensional bubble length (L_b/D) has been shown. It may also be noted that the value of Fr obtained from the analytical model matches with the asymptotical value of the numerical results.

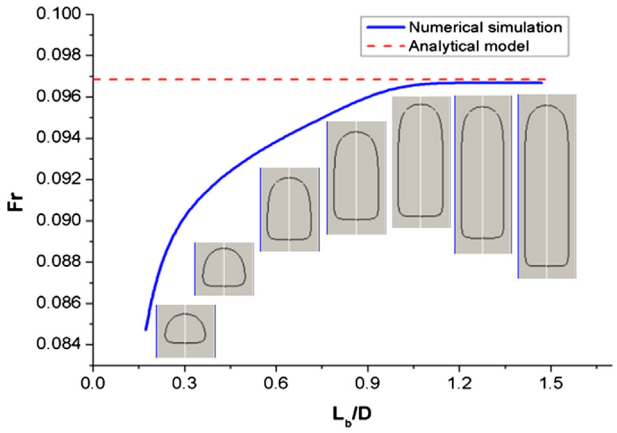

Fig. 3. Plot of Fr vs length of the bubble. The tube diameter for these simulations is 2 cm, K = 0.33 and n = 0.96.

The numerical study has been performed for a wide range of bubble volume. Once the nose shape develops for a Taylor bubble, the buoyant force due to the increase in bubble length (volume) is balanced by the increase in viscous drag and hence the terminal velocity of the bubble becomes independent of its volume.The same has also been observed for bubble motion through Newtonian fluids and the present case is also not an exception.

However the present exercise provides some additional information. The case study clearly depicts how the bubble shape and velocity changes gradually to reach their respective asymptotic values. It also indicates that for the present operating condition the rise velocity of the Taylor bubble may be considered constant beyond a value of $L_b/D = 1.0$.

3.3. Velocity profile and tail vortices

The flow field around the nose of the Taylor bubble is shown in Fig. 4(a) for a typical value of K = 1.621 and n = 0.496, which corresponds to the properties of 0.8% CMC solution. We have shown only the velocity field outside the bubble. As we can see from the flow field, the gas bubble rises upward and pushes the liquid, in front of the nose, up and away from the center of the tube. For other values of K and n the qualitative trend of the velocity field remain unchanged. In Fig. 4(b) we have shown the plot for instantaneous axial velocity profile at the cylindrical body of the bubble with respect to non-dimensional radial coordinate (r/D). The instantaneous velocity has been calculated at a distance of 1.2D below the tip of the bubble nose. The velocity of the gas inside the bubble is upward while the liquid film falls downward. The liq-

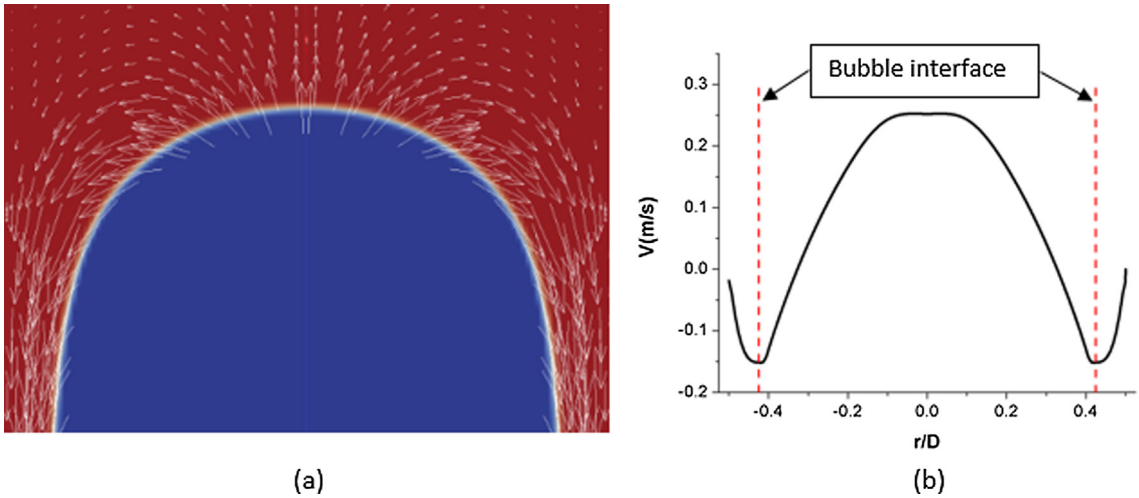

Fig. 4. Velocity field of the Taylor bubble rising in 0.8% CMC solution: (a) Flow field around the nose of the bubble (b) instantaneous axial velocity profile at a distance 1.2D from the tip of the bubble.

uid that is pushed away near the nose of the bubble forms the falling liquid film (Fig. 5).

An elaborate study on the tail vortices of taylor bubble in Newtonian fluid has been done by Campos and Carvalho (1988) and Nogueira et al. (2006). In Campos and Carvalho (1988), a nondimensional number $N_f = \rho_L(gD^3)^{\frac{1}{2}}/\mu_L$ has been introduced to characterize the wake of the Taylor bubble. It has been shown that for $N_f < 500$, the flow around the bubble is axisymmetric and laminar.

For analyzing the tail vortices in power law fluid, we have used a dimensional version of N_f by replacing μ_L by K. Thus

$$N_f = \frac{\rho_L(gD^3)^{\frac{1}{2}}}{K}$$

Campos and Carvalho (1988) experimentally demonstrated that the liquid flow remains laminar and the bubble is axisymmetric when $N_f < 500$. It may be noted that the in all our simulations, the estimated value of N_f is below 500 which justifies the assumptions made.

3.4. Effect of power law parameters on the shape and motion of Taylor bubble

We have used the Froude number (Fr) to study the change in terminal velocity. Froude number gives the relative strength between inertia and gravitaional forces($Fr = V_b/\sqrt{(gD)}$), where V_b is the terminal velocity of the bubble and D = 2 cm is the tube daimeter. We have taken six different values of n starting from n = 0.6 to 1.5 and three different values of K which are 0.2, 0.33 and 0.4.

From Fig. 6 it is clear that as K increases, the terminal velocity decreases due to an increase in the effective viscosity of the liquid and as n increases the terminal velocity decreases as well. The power law index n has a pronounced effect on the bubble velocity particularly in the shear thinning region ($n < 1$). Similarly the decrease in velocity due to an increase in the magnitude of K is more observable in the shear thinning region compared to the shear thickening region. To understand the reason of the above trend of bubble velocity, we explore the sensitivity of the effective viscosity of the power law fluid with respect to n and K. For that, from the expression of μ_{eff} given in Eq. (24), we estimate $\frac{d\mu_{eff}}{dK}$ and $\frac{d\mu_{eff}}{dn}$, which are the sensitivities with respect to K and n respectively. We found out that the value of $\frac{d\mu_{eff}}{dn}$ for different combinations of n and K is much higher than that of $\frac{d\mu_{eff}}{dK}$ in the shear thinning region, whereas their values are comparable in the shear thickening region. Thus, with the increase in n, the viscosity increases much rapidly than that with K for $n < 1$. Therefore, the sharp decrease in the value of Fr with n compared to that with K in the shear thinning domain is not unexpected. For $n > 1$, the increase in viscosity for an increase in both n and K are almost similar resulting in a similar decrease in bubble velocity (Fr).

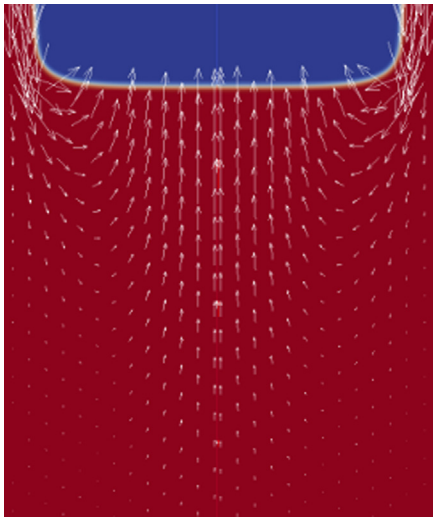

Fig. 5. Tail vortices of the Taylor bubble rising in 0.8% CMC solution. The velocity vector plot has been done with respect to a fixed reference frame.

We also tried to find an explanation for the effect of power law parameters from our analytical model. Assuming the equilibrium film thickness to be almost a constant and then simplifying Eq. (26), we get that for a power law fluid

$$Fr \quad \sim \quad \frac{\sqrt{D}}{K^{\frac{1}{n}}} \tag{30}$$

Here we see that, in the above expression, the exponent of K is the reciprocal of n. This gives us an understanding about why there is a strong influence of n in the shear thinning region. Due to the presence of $1/n$ term in the expression of Fr, the value of n has a pronounced effect on the bubble velocity for $n < 1$. Whereas, for $n > 1$, a change in n will not affect the velocity so much.

Besides validating the maximum bubble radius $(r/D)_{max}$ with experimental data, we have also studied the bubble shape for different values of n and K. In Fig. 7(a) the variation of bubble shape with K has been shown and in Fig. 7(b) the dependence on n value has been plotted. The origin of the coordinate axes is at the tip of the bubble.

One may note that the shape of the bubble does not show any perceivable change with respect to K but it changes with n. The film thickness increases with the increase in n. This is primarily due to the sensitivity of the effective viscosity of the surrounding liquid with respect to n and K. Since, in the shear thinning region, the magnitude of $\frac{d\mu_{eff}}{dn}$ is much higher than $\frac{d\mu_{eff}}{dK}$, the viscosity of surrounding liquid increases rapidly with n than with K, the bubble becomes slender and the thickening of the film happens. On the other hand, the small change in viscosity with K does have a notable effect on the film thickness.

3.5. Effect of surface tension

By changing the surface tension its effect on bubble velocity and shape has been analyzed. The Bond number or Eötvös number ($Eo = \frac{(\rho_L - \rho_G)gD^2}{\sigma}$) gives the relative strength of buoyancy and surface tension forces. Here ρ_L is the density of the liquid phase, ρ_G is the density of the gaseous phase, D is the diameter of the tube which in this case has been kept constant at 2 cm and σ is the surface tension. We have varied the value of σ from 0.02 to 0.08 N/m.

The surface tension has almost a negligible effect on the bubble velocity but it affects the level of concavity of the Taylor bubble tail significantly. In Fig. 8 the tail shape of the Taylor bubble for three different Bond number have been depicted. At a low value of surface tension the inertial force becomes dominant and the interface deforms more. The interface becomes concave to convex with a decrease in the value of Eo. We also studied the effect of surface tension on the nose shape of the Taylor bubble and found no significant variation. The bubble velocity is influenced by the shape of the bubble nose while the shape of the wake affects the tail vortices. Since there is no observable change in the nose shape, so the terminal velocity of the Taylor bubble remains unaffected by the change in surface tension within the range of our investigation.

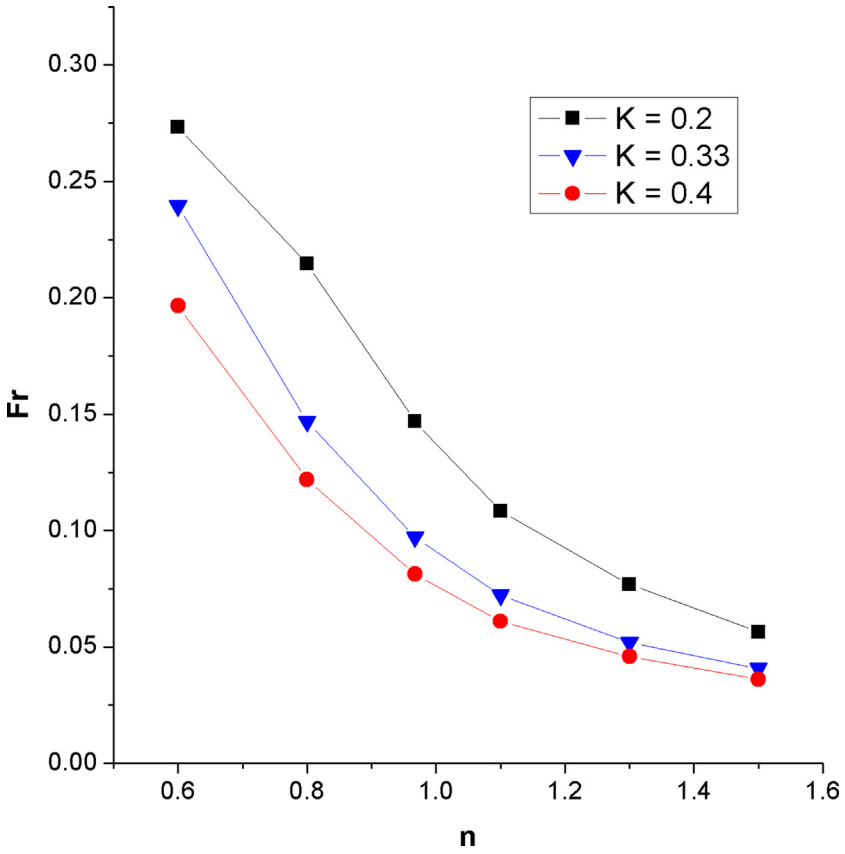

Fig. 6. Effect of n and K on *Fr*. Tube diameter is D = 2 cm.

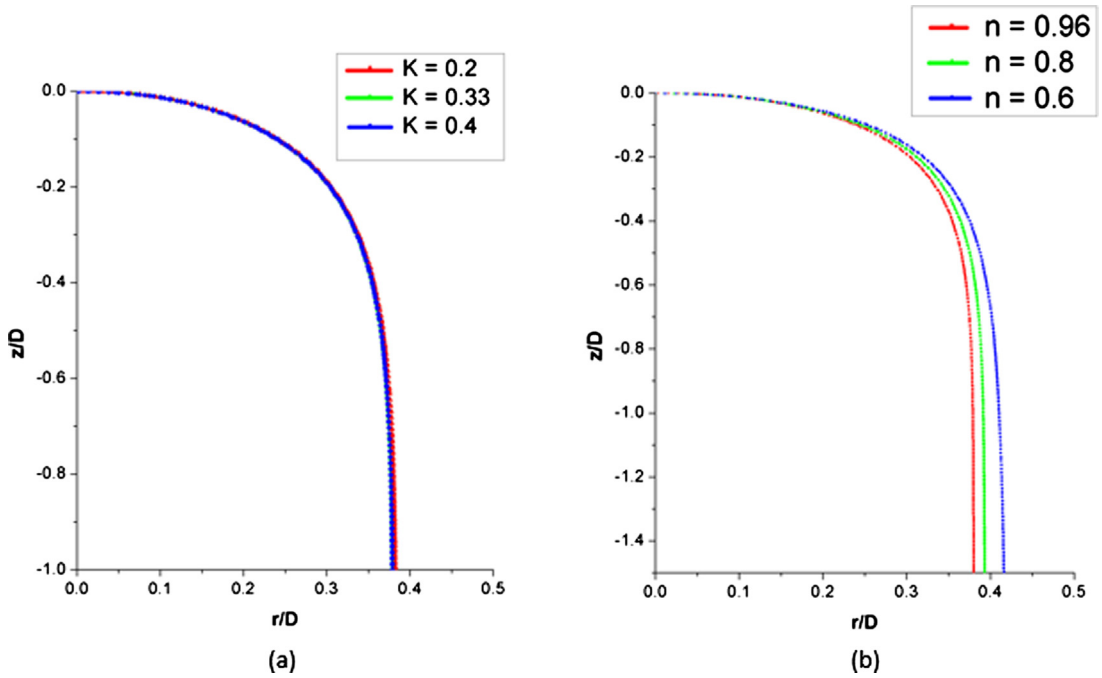

Fig. 7. Effect of power law parameters on bubble shape: (a) Bubble shape has been plotted for different values of K with n = 0.96 (b) Shape of the bubble for different n at a constant K value of 0.33.

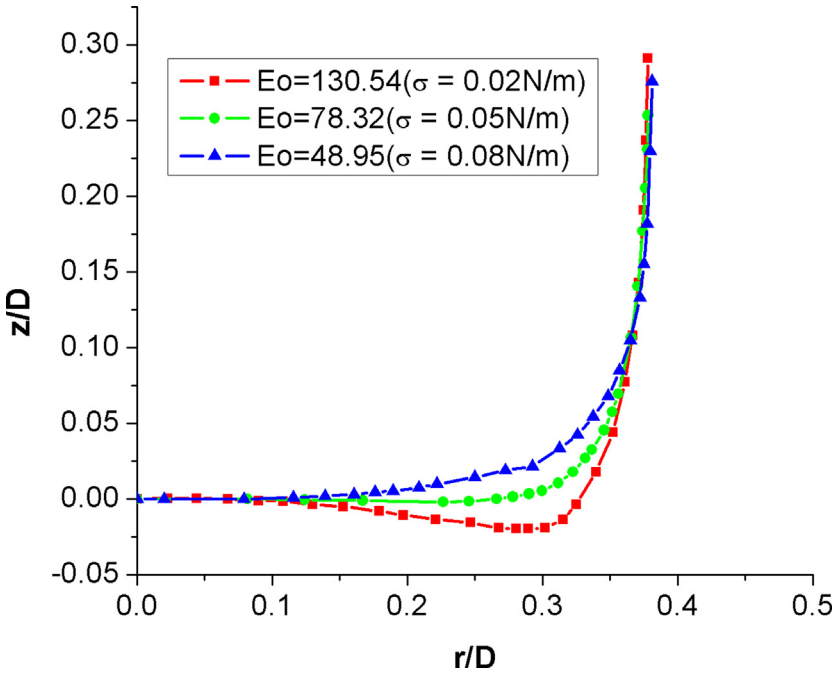

Fig. 8. Effect of surface tension on the tail shape of the Taylor bubble. K = 0.33 and n = 0.96.

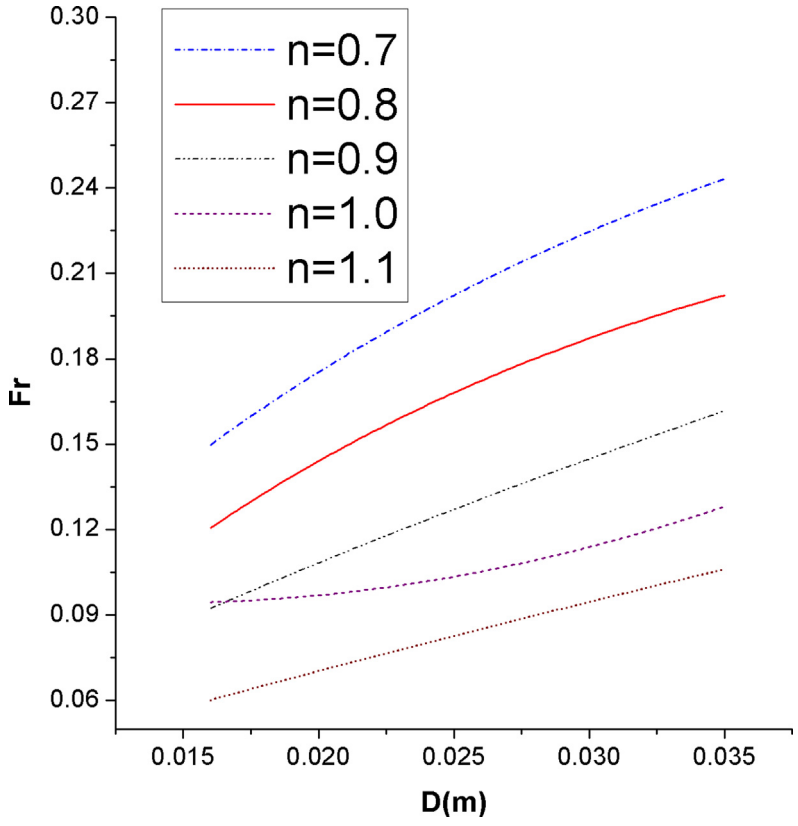

Fig. 9. Effect of tube diameter D on Fr. For this study K has been kept constant at 0.33.

3.6. Effect of tube diameter

For different tube diameters, the terminal velocity of the Taylor bubble in power law fluid has been calulated. We have obtained the bubble velocity for shear thinning($n < 1$) as well as shear thickening($n > 1$) fluids. We also simulated the rise of the Taylor bubble in the Newtonian fluid($n = 1$) for the sake of comparison. The results are shown in Fig. 9. We have used Froude number (Fr) to study the influence of tube diameter on bubble velocity.

We have made the simulations for five different diameters from 1.6 cm to 3.5 cm. With the increase in tube diameter, the viscous forces decrease and the terminal velocity of the bubble increases.

As we can see from the plot, all the curves are concave downward except for the Newtonian fluid i.e. $n = 1$. For the Newtonian fluid the curve is marginally concave upward. This indicates the difference in the flow dynamics between a power law and a Newtonian fluid.

To understand this behaviour, we use our analytical expression. As mentioned in Section 3.4, upon simplification of Eq. (26), for a power law fluid,

$$Fr \sim \frac{\sqrt{D}}{K^{\frac{1}{n}}} \tag{31}$$

Also, upon simplifying the correlation given by Llewellin et al. (2012) we find that for a Newtonian fluid,

$$Fr \sim D^{1.54} \tag{32}$$

Since the exponent of D for power law fluid is less than 1, we see that the curves of Fr vs D for power law fluid to be concave downward. Whereas, for a Newtonian fluid, the exponent of D is greater than 1 and as such for Newtonian fluid the curve is concave upward.

Another important point to mention is that, with the increase in tube diameter, the value of Fr increases for the power law fluids. This is due to the dominance of the inertial forces. As for the Newtonian fluid, there is a rise in Fr with D. This deviates from the analytical models where, for constant viscosity, the Froude number is independent of tube diameter. One possible reason behind such deviation is the high viscosity of the fluid. The analysis of this particular phenomena is beyond the scope of the work presented here and can be taken up in the future for further study.

3.7. Conclusion

In this paper, we attempt to predict theoretically the dynamics of Taylor bubbles through circular tubes filled with power law fluids. The free ware OpenFOAM has been used to predict the shape and velocity of the rising axisymmetric Taylor bubbles. Conservation equations based on one field approach and VOF for interface capturing has been used. Parallelly, a semi-analytical approach has been made to find out the rise velocity considering viscous drainage of liquid through the film surrounding the bubble. The method yields a closed form expression for the rise velocity using a single tuning coefficient from experimental data. The rise velocity obtained from numerical simulation and semi-analytical theory exhibit a close agreement with the experimental results for different values of K and n of the power law fluid.

The film thickness predicted from the computational simulation, matches with the experimental data. Out of available correlations for film thickness, the one by Brown (1965) compares with the experimental values when Newtonian viscosity is replaced by effective viscosity of the power law fluid. As through a Newtonian fluid, the rise velocity of bubble increases also through power law fluids as its volume increases. Eventually, the bubble assumes the shape of a Taylor bubble and the rise velocity reaches a constant value asymptotically for a particular fluid. Though the rise velocity is dependent on both K and n of a power law fluid, it is more sensitive to n. In fact this is also corroborated by the change of nose curvature as n increases. However, notionally an increase in viscosity decreases the rise velocity and increases the slenderness of the Taylor bubble through a non-Newtonian fluid as is also observed for a Newtonian fluid. The surface tension on the other hand has no noticeable effect on the rise velocity and nose shape of the bubble while it influences the shape of the tail to some extent.

The power law fluids considered for the present study possess high value of viscosity. In the same range of viscosity the rise velocity of Newtonian fluid has also been computed numerically. At this range of viscosity the Froude number varies with diameter. An explanation for this difference can be given from existing correlation proposed by Llewellin et al. (2012).

The semi-analytical model and the numerical results have been compared with the limited available experimental data for rising Taylor bubbles in four different diameters through power law fluid with various combinations of n and K. Further study on the bubble dynamics for different power law fluids with known n and K values needs to be done.

References

Arajo, J., Miranda, J., Campos, J., 2017. Taylor bubbles rising through flowing non-newtonian inelastic fluids. J. Nonnewton. Fluid Mech. 245, 49–66.

Batchelor, G., 1987. The stability of a large gas bubble rising through liquid. J. Fluid Mech. 184, 399–422.

Batchelor, G.K., 2000. An Introduction to Fluid Dynamics. Cambridge University Press.

Bendiksen, K.H., 1985. On the motion of long bubbles in vertical tubes. Int. J. Multiphase Flow 11 (6), 797–812.

Brackbill, J., Kothe, D., Zemach, C.A., 1992. continuum method for modeling surface tension. J. Comput. Phys. 100 (2), 335–354.

Brown, R.A.S., 1965. The mechanics of large gas bubbles in tubes: I. bubble velocities in stagnant liquids. Canad. J. Chem. Eng., vol. 43, 5 (10), pp. 217–223.

Bugg, J., Mack, K., Rezkallah, K.A., 1998. numerical model of Taylor bubbles rising through stagnant liquids in vertical tubes. Int. J. Multiph. Flow 24 (2), 271–281.

Campos, J.B.L.M., Carvalho, J.R.F.G.D., 1988. An experimental study of the wake of gas slugs rising in liquids. J. Fluid Mech. 196, 27–37.

Carew, P., Thomas, N., Johnson, A.A., 1995. physically based correlation for the effects of power law rheology and inclination on slug bubble rise velocity. Int. J. Multiph. Flow 21 (6), 1091–1106.

Collins, R., De Moraes, F., Davidson, J., Harrison, D., 1978. The motion of a large gas bubble rising through liquid flowing in a tube. J. Fluid Mech. 89 (3), 497–514.

Davies, R., Taylor, S.G., 1988. The mechanics of large bubbles rising through extended liquids and through liquids in tubes. Dynam. Curved Fronts Elsevier, 377–392.

Dumitrescu, D.T., 1943. Strömung an einer luftblase im senkrechten rohr. ZAMM-J. Appl. Math. Mech./Zeitschrift für Angewandte Mathematik und Mechanik 23 (3), 139–149.

Figueroa-Espinoza, B., Fabre, J., 2011. Taylor bubble moving in a flowing liquid in vertical channel: transition from symmetric to asymmetric shape. J. Fluid Mech. 679, 432–454.

Funada, T., Joseph, D., Maehara, T., Yamashita, S., 2005. Ellipsoidal model of the rise of a Taylor bubble in a round tube. Int. J. Multiphase Flow 31 (4), 473–491.

Goldsmith, H.L., Mason, S.G., 1962. The movement of single large bubbles in closed vertical tubes. J. Fluid Mech. 14 (1), 42–58.

Hirt, C., Nichols, B., 1981. Volume of fluid (vof) method for the dynamics of free boundaries. J. Comput. Phys. 39 (1), 201–225.

Kaml, F., 2003. Free coating of a non-Newtonian liquid onto walls of a vertical and inclined tube. Chem. Eng. Process. 42 (7), 569–581.

Kang, C.-W., Quan, S., Lou, J., 2010. Numerical study of a Taylor bubble rising in stagnant liquids. Phys. Rev. E 81 (6). 066308.

Llewellin, E., Del Bello, E., Taddeucci, J., Scarlato, P., Lane, S., 2012. The thickness of the falling film of liquid around a Taylor bubble. Proc. R. Soc. A 468 (2140), 1041–1064.

Lu, X., Prosperetti, A.A., 2009. numerical study of Taylor bubbles. Industr. Eng. Chem. Res. 48 (1), 242–252.

Mandal, T.K., Das, G., Das, P.K., 2008. Liquid Taylor bubbles rising in a vertical column of a heavier liquid: an approximate analysis. J. Fluids Eng., vol. 131, 1, pp. 011303–011303–7.

Mao, Z.-S., Dukler, A., 1990. The motion of Taylor bubbles in vertical tubes. I. A numerical simulation for the shape and rise velocity of Taylor bubbles in stagnant and flowing liquid. J. Comput. Phys. 91 (1), 132–160.

Mukundakrishnan, K., Eckmann, D.M., Ayyaswamy, P., 2009. Bubble motion through a generalized power-law fluid flowing in a vertical tube. Ann. N. Y. Acad. Sci. 1161 (1), 256–267.

Nogueira, S., Riethmuler, M., Campos, J., Pinto, A., 2006. Flow in the nose region and annular film around a Taylor bubble rising through vertical columns of stagnant and flowing Newtonian liquids. Chem. Eng. Sci. 61 (2), 845–857.

Nogueira, S., Riethmuller, M., Campos, J., Pinto, A., 2006. Flow patterns in the wake of a Taylor bubble rising through vertical columns of stagnant and flowing newtonian liquids: an experimental study. Chem. Eng. Sci. 61 (22), 7199–7212.

Reinelt, D., 1987. The rate at which a long bubble rises in a vertical tube. J. Fluid Mech. 175, 557–565.

Rusche, H., 2002. Computational Fluid Dynamics of Dispersed Two-phase Flows at High Phase Fractions PhD thesis. Imperial College London.

Sousa, R., Pinto, A., Campos, J., 2006. Effect of gas expansion on the velocity of a Taylor bubble: Piv measurements. Int. J. Multiph. Flow 32 (10), 1182–1190.

Sousa, R., Riethmuller, M., Pinto, A., Campos, J., 2005. Flow around individual Taylor bubbles rising in stagnant cmc solutions: Piv measurements. Chem. Eng. Sci. 60 (7), 1859–1873.
Viana, F., Pardo, R., Ynez, R., Trallero, J.L., Joseph, D.D., 2003. Universal correlation for the rise velocity of long gas bubbles in round pipes. J. Fluid Mech. 494, 379–398.
Wallis, G. General correlations for the rise velocity of cylindrical bubbles in vertical tubes.
White, E., Beardmore, R., 1962. The velocity of rise of single cylindrical air bubbles through liquids contained in vertical tubes. Chem. Eng. Sci. 17 (5), 351–361.
Zudin, Y.B., 2013. Analytical solution of the problem of the rise of a Taylor bubble. Phys. Fluids 25 (5). 053302.
Zukoski, E., 1966. Influence of viscosity, surface tension, and inclination angle on motion of long bubbles in closed tubes. J. Fluid Mech. 25 (4), 821–837.